



Overview of spatial and timing resolution of event counting detectors with Microchannel Plates

A.S. Tremsin^{*}, J.V. Vallerga, O.H.W. Siegmund

Space Sciences Laboratory, University of California at Berkeley, Berkeley, CA 94720, USA



ARTICLE INFO

Keywords:

Event counting detectors
High resolution
Microchannel Plates
High dynamic range
Low noise

ABSTRACT

Event counting detectors with Microchannel Plates (MCPs) rely on conversion of incoming particles (photons, electrons, neutrons, atoms, ions) into an output charge of 10^3 – 10^7 electrons. This signal multiplication enables operation of those detectors at virtually zero readout noise and at very low input fluxes. The encoding of event position and timing can be performed by various types of readout configurations, which need to be selected for a particular experiment. Substantial developments in microelectronics have extended the capabilities of MCP counting detectors to GHz rates, increased their formats to 20 cm and allowed detection of multiple simultaneous events with spatial and timing resolution as good as ~ 10 μm and ~ 10 – 20 ps, respectively. Unfortunately not all these characteristics are available in a single device. A brief overview of performance characteristics of event counting MCP detectors with different readouts is presented in this paper, providing the guidance for the selection of a particular detector configuration for a given set of experimental requirements.

Contents

1. Introduction	1
2. The principle of MCP detector operation	2
2.1. Timing signal in detectors with microchannel plates	2
3. Performance of MCP detectors with different readout configurations	3
3.1. MCP detectors with phosphor screen	3
3.2. Readouts with charge division encoding	4
3.3. Charge propagation encoding readouts	5
3.4. Multi-anode and pixelated readouts	7
4. Summary	9
Acknowledgments	10
References	10

1. Introduction

Event counting detectors with Microchannel Plates [1] (MCPs) have niche applications where the capability of MCPs to multiply electrons to an output charge of 10^3 – 10^7 electrons enables high resolution particle detection with virtually no noise events generated by the readout electronics. The fact that signal multiplication is spatially constrained to a single MCP pore (several pores in case of several MCPs stacked for higher gain) allows event encoding with spatial resolution limited by the distance between the pores (typically 6–12 μm for the current MCP technology). The transit time spread of output charge depends on the size of the pore and is typically ~ 10 – 25 ps for 5–10 μm pores [2,3], and ~ 50 – 100 ps for 40 μm pores [4]. No event after-pulsing

generated by the MCP stack and relatively low dark count rate of < 0.1 count/ cm^2/s [5] enable operation at high dynamic range (~ 0.1 – 10^7 counts/ cm^2/s), allowing detection of very low and relatively high input fluxes in one image, providing the detector readout is capable of operation at high local counting rates. Detection efficiency of MCP devices is also relatively high and it depends on the efficiency of conversion of the incoming particle into an electron or several electrons at the MCP input (as in the case of visible, UV or soft-X-ray photon, ion, neutral detection) or within the bulk of MCP glass (as in case of neutron or X-ray and gamma photon detection). Photon detection efficiency of bare MCPs [6] can be enhanced by the application of various types of photocathodes which increase the sensitivity to visible, UV and soft

^{*} Corresponding author.

E-mail address: ast@ssl.berkeley.edu (A.S. Tremsin).

X-ray photons [7,8]. Incoming ions and electrons can be accelerated to reach nearly 100% detection efficiency as various techniques can be used to steer all secondary electrons, including the ones produced in between the pores, into an adjacent MCP pore. Doping the MCP glass with ^{10}B and Gd atoms made them sensitive to cold, thermal and epithermal neutrons [9,10]. Once the incoming particle is converted into an easily measurable charge of 10^3 – 10^7 electrons the event position and timing can be encoded by a readout anode, which is usually positioned at ~ 0.5 – 15 mm distance from the MCP output surface, depending on the specific type of readout configuration. The capabilities of MCP electron amplifiers mentioned above have to be matched by the performance of readout electronics, which has seen a substantial evolution over the last few decades. Unfortunately there is no best type of readout providing all the best detection characteristics in one device. Some compromises between the spatial and timing resolution, counting rate capabilities, active area size, multi-hit capability and other parameters have to be found for a particular event counting application. In addition to traditional single-pixel photomultipliers, there are many alternative (and probably better or more suitable) technologies for single pixel or small array event counting, which were developed recently due to the tremendous progress in microelectronics. Among recently developed solid state detection devices are silicon photomultipliers (Si PMTs) [11], single photon avalanche photodiodes (SPADs) [12,13] and others. The possibility to perform high resolution imaging with sub-ns timing resolution, low dark noise and large dynamic range make MCP-based devices still attractive for some applications, despite some of the complications related to MCP technology, such as the requirement to operate in vacuum, high voltage applied to MCPs (typically ~ 1 kV per microchannel plate), limits on local count rate (determined by the pore recharge time), fixed pattern distortions at multifiber boundaries, and few others.

In this article we provide a brief overview of different readout technologies for the MCP imaging detectors and compare their spatial and temporal resolution. Only multi-pixel MCP imaging devices are considered here, where image formats larger than 256×256 pixels are available.

2. The principle of MCP detector operation

The principle of MCP detector operation is schematically shown in Fig. 1. The incoming particle is converted into an electron (in case of photons by a photocathode deposited directly onto the MCP or on the input window), which is then subsequently amplified by the MCP or a stack of two or three MCPs to an output charge of 10^3 – 10^7 electrons, emitted towards the readout, encoding event location and timing. The MCP are produced such that the pore axis is typically biased at 8–12 degree angle relative to the surface normal. Two or three plates are mounted in the detector such that the pore tilt is in the opposite direction in each consecutive plate, as shown in Fig. 1 for a “chevron” pair, while 3-plate stacks are often referred to as “Z-stack” configuration. These MCP stacking geometries prevent the ions generated by residual gas ionization by output electrons to be accelerated towards the MCP input surface, where they can produce noise events. The event amplification within the MCP pore is physically restricted to that pore, which received the initial electron produced by the incoming particle. In case of multiple MCPs used in a stack several adjacent pores are stimulated by the electrons emitted from the previous MCP. The center of the output charge still corresponds to the location of the initial MCP pore exited by the incoming particle, thus allowing an accurate event encoding limited by the MCP geometry (i.e. by the distance between two adjacent pores). The extracted charge from the pore needs to be resupplied before the next event can be properly detected and that recharge time can limit the local count rate capability of the entire detector. The higher the gain needed for the detector operation, the longer is the MCP recharge time. Microchannel plates with low resistance values are usually used for the devices

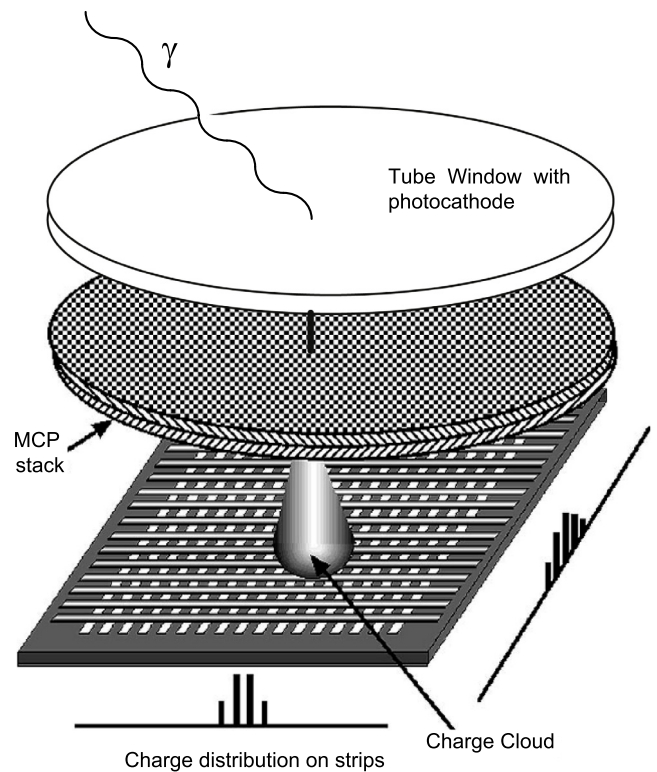


Fig. 1. Schematic representation of a detector with a “chevron” stack of microchannel plates. A semitransparent photocathode is deposited on the input window in that configuration. An open-face detector can be facing vacuum chamber with no window installed in front of it. The photoelectron (in case of photon detection) or secondary electrons produced by an ion, incoming electron or neutron are amplified with gain 10^3 – 10^7 . The resulting charge is collected by a readout (Cross Strip anode is shown in that figure). The event position (and in some configurations event timing) is encoded by the readout.

requiring operation at high counting rates, but the MCP resistance cannot be much lower than ~ 10 M Ω for an MCP with ~ 10 cm 2 active area due to thermal runaway caused by the negative thermal coefficient of MCP resistance.

2.1. Timing signal in detectors with microchannel plates

The timing of each registered event in a detector with microchannel plates can originate in two locations in the detector: at the exit electrode of the MCP stack or at the readout anode itself, as schematically shown in Fig. 2. There are certain advantages and disadvantages of each. Emission of an electron cloud by the MCP stack creates an induced pulse of positive polarity on the output electrode, which is proportional to the gain of that event. That fast pulse is followed by a relatively slow recovery of the charge, enabling event timing to be picked up through a capacitive coupling to the output electrode. The initial positive pulse at the MCP electrode intrinsically is very fast and if measured properly can be as accurate as the limit of MCP timing resolution, namely transit time spread of electron multiplication within the pore(s). However, the output MCP electrode is not a good transmission line and charge propagation along the electrode can be affected by the interference from multiple reflections at the MCP periphery. Some users coat the output electrode with gold or high conductivity metal and even isolated stripes to get fast timing in specific areas. One of the strongest deficiencies of measurement timing at the output electrode is the difficulty of measuring timing of multiple events occurring nearly simultaneously or with a short time interval between them. These signals from individual events will interfere with each other and are difficult to distinguish and to process

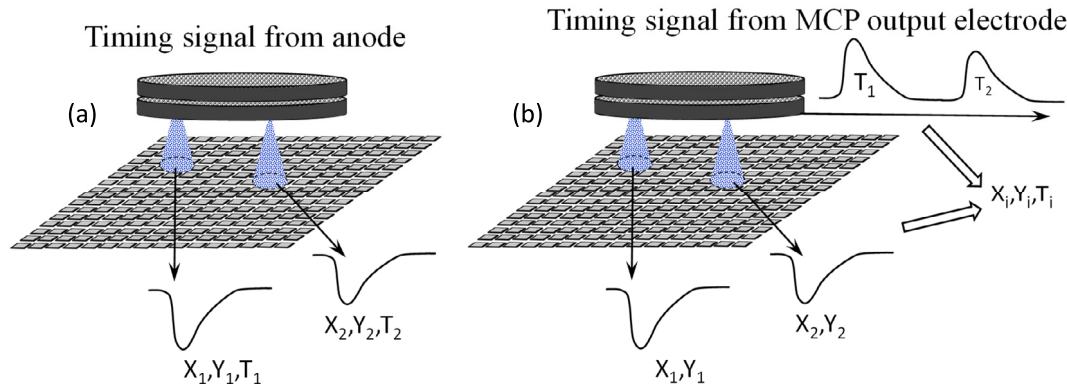


Fig. 2. (a) The timing of the event is encoded by the readout. A pixelated readout is shown in this figure, where each pixel registers both position and time of incoming particle. Multiple simultaneous events can be processed. (b) The timing of the event is registered by the positive pulse appearing at the MCP output electrode when an electron avalanche leaves the MCP. Two data streams (position X_i , Y_i from the anode) and time T_i from the MCP output need to be synchronized. Incoming particles should be separated in time to allow an accurate measurement of their time of arrival.

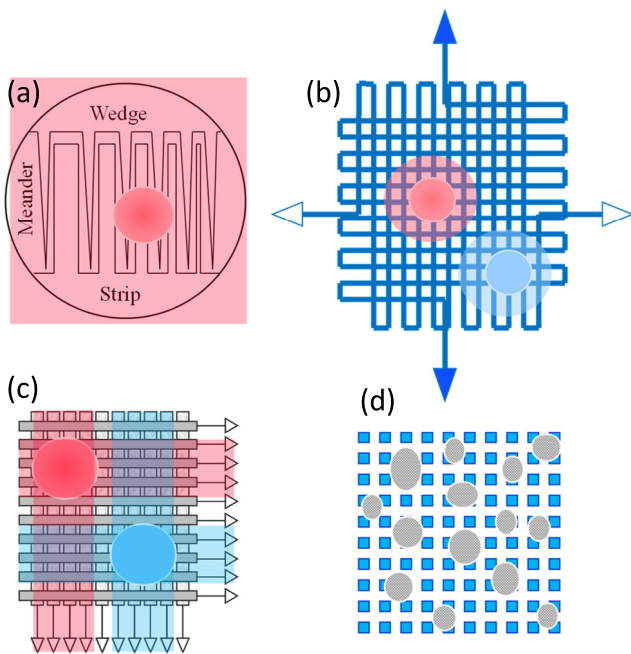


Fig. 3. Various types of event encoding readouts. (a) Wedge Strip Zig (WSZ) charge division readout. Only 3 electrodes/amplifier channels are used. One event is processed at a time. (b) Cross Delay Line (XDL) charge propagation readout. 4 fast amplifiers measuring time delay between the pulses at each end of two orthogonal delay lines. Several spatially separated events can be detected (MCP output electrode signal is used to resolve ambiguity between the fast signals (Section 3.3)). (c) Cross Strip (XS) readout. Multiple charge sensitive amplifiers are used in the readout (one per strip). Event location is encoded by calculation of center of charge distribution in two orthogonal sets of strips. Several spatially separated events can be registered. (d) Pixelated readout. Independently operating pixels allow detection of many simultaneous events.

properly, especially taking into account the fact that the gain of MCPs is not a constant value and it has some finite statistical fluctuation from one event to another. Another challenge in that configuration, specifically difficult at high input rates, is the need to synchronize the two independent data streams: one for the timing of registered events and the other for the (X, Y) position. Ideally time encoding at the readout anode would be a better choice for the detection at high counting rates or for the measurements of nearly simultaneous events. A pixelated readout with many independently operating pixels can process many nearly simultaneous events and measure both spatial and temporal parameters of each registered particle. However, the charge spread in the gap between the readout and the MCP stack

may spatially broaden the pulse at the anode, thus effectively reducing signal to noise ratio at the anode. Moreover, many charge division and charge propagation readouts cannot measure event timing accurately as pulse propagation in those readouts introduces additional distortions. A single pixel anode with a matching 50 Ohm output impedance, as reported in reference [14] can be a good alternative for high resolution timing, but here we only consider imaging detectors providing both spatial and temporal information on each registered particle. For the reasons mentioned in this section, most charge division and charge propagation readout configurations rely on the timing signal picked up at the MCP output electrode, as shown in Fig. 2b. The same timing reconstruction from the induced pulse at the MCP output electrode is used for the devices where timing resolution of the pixelated readout is not sufficiently high, as in the case of Timepix Readout Integrated Circuit (ROIC) with its limited 10 ns timing accuracy [15].

3. Performance of MCP detectors with different readout configurations

Various types of event encoding readouts can be used in MCP detectors, depending on the priorities and requirements for a particular application. The MCP output charge can be converted into visible light photons by a phosphor screen placed just below the MCPs, and subsequently detected by a photon imaging device. The timing resolution of such devices is usually rather low or limited to a stroboscopic mode of operation in case of ns-scale timing resolution requirement. The location of incoming particle can also be determined by the position of the pads which receive output charge exceeding a threshold level, as it is performed by multianode MCP photomultipliers (MCP PMTs) [16] which are limited to <1000 pixels and require many electronics channels. A much higher spatial resolution can be reconstructed through a charge division or charge propagation methods used in certain anodes (see Sections 3.2 and 3.3). Finally, different ROIC chips can be placed behind the MCP, with many independently operating pixels, allowing detection of a large number of simultaneous events, Section 3.4.

3.1. MCP detectors with phosphor screen

One of the possible readouts can be a phosphor screen, which converts the MCP output charge into visible light (often such configuration is referred to as an image intensifier). The timing resolution in such devices is determined by the photon detectors coupled to the phosphor screen, which usually do not take full advantage of sub-ns timing resolution of MCP event amplification. One of the crucial parameters limiting the time resolution of such systems is the phosphor decay time (fluorescence lifetime, typically ~ 1 ms and ~ 300 ns for widely used P43 and P46 phosphor screens, respectively). A stroboscopic imaging

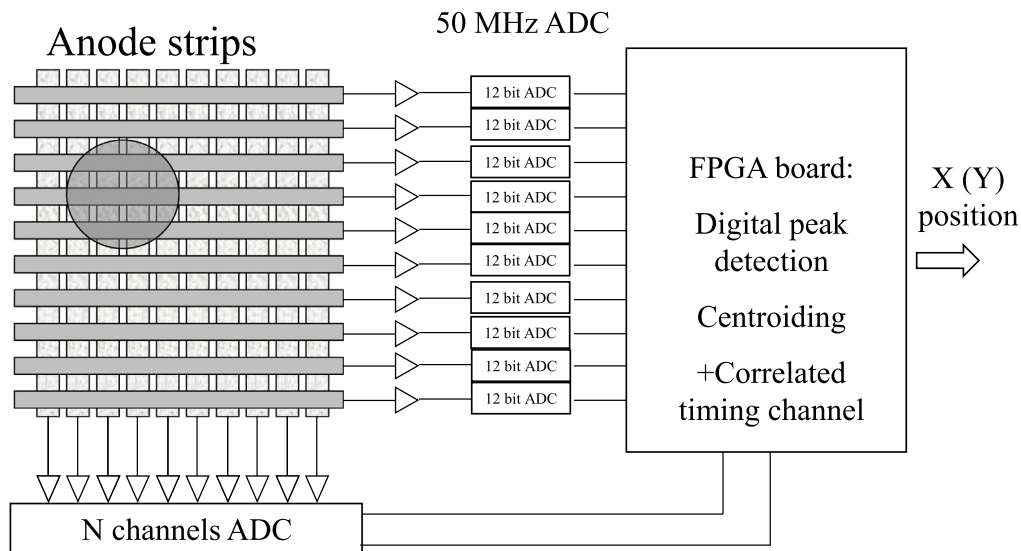


Fig. 4. Cross Strip charge division readout. The charge collected in each strip is amplified and digitized in parallel. An FPGA board performs event detection and calculates the center of each event from measured charge distribution in two orthogonal sets of fingers. Coincidence between X and Y channels is used to combining them into event position. Event timing can also be measured from the pulse generated by the charge collected by the strips with an accuracy of ~ 1.1 ns (Section 3.2).

can be performed with such hybrid detectors where photocathode can be time-gated with a ns accuracy and a large number of simultaneous events can be detected in one single frame. However, such devices are not event counting and after each gated frame require a substantial amount of time for the frame readout by an image integrating Charge Coupled Device (CCD) or a Complementary Metal Oxide Semiconductor (CMOS) sensor. The spatial resolution of such devices can be on the scale of $\sim 100\text{--}200$ μm [17] with no event centroiding and can be as good as distance between the MCP pores when event centroiding is applied [18], but that can be performed at rather limited rates at present time.

Detectors with microchannel plates coupled to a phosphor screen found wide use in many applications including imaging at very low light fluxes [19], astrophysics instrumentation [20], detection of fast [21] and thermal neutrons [22] to name the few, and many others. All these devices are typically not counting single particles, although they can do that in case the input fluxes are quite low.

Single particle detection was enabled recently by a very interesting development of a hybrid detector, where events produced on the phosphor screen of an image intensifier are readout by an event counting system Timepix/Timepix3 ROICs with a light sensitive Si sensor [23]. The capability of this system to count individual events with 1.56 ns timing resolution (with Timepix3 ROIC [24]) enabled high resolution measurements in electron and ion detection and phosphorescence lifetime imaging [25,26].

3.2. Readouts with charge division encoding

Encoding of the event position from the ratio of charges collected by the anode electrodes has been used in various MCP detectors due to the relatively simple electronics with very few amplification channels required, in particular only 3 channels for Wedge /Strip /Zig anodes [27,28], Fig. 3a, 4 channels for the resistive anodes [29] and 6–9 channels for the Vernier anodes [30]. Optimization of the electrode capacitance is required for such anodes as the accuracy of measured charge value in such readouts decreases with the larger capacitance of the individual electrodes [31]. Among the benefits of charge division readouts are their relative simple planar electrode geometry, making them relatively easy to manufacture with basic lithographic etching of metals deposited on the materials compatible with the vacuum levels required for the MCP detectors, including sealed tube devices. There are many possible charge division configurations, including the ones where

radial coordinates are measured [32,33]. The number of simultaneous events detected by a charge division readouts is typically restricted to one as accurate charge value collected by each electrode is required for the reconstruction of event position in these readouts. The count rate in such detectors is usually limited to <1 MHz level, which is determined by the shaping time (typically $\sim \mu\text{s}$) in the charge sensitive amplifiers, which is relatively large in order to minimize the electronic baseline noise.

Among the most recent developments of charge division readouts is the Cross Strip (XS) anode, where charges from multiple individual strips are digitized at high rates and the event location is found from the center of gravity of measured projections on charge distribution on two axes [34,35], Fig. 4. A large number of amplification channels, compared to other charge-division schemes, is implemented in XS devices with a multichannel Application Specific Integrated Circuit (ASIC) followed by digitization, as shown in Fig. 4. A self-triggered electronics mode can function when strip charges are stored in a ring buffer and the ADC only digitizes adjacent channels for the events exceeding a preprogrammed threshold value [36]. The use of dedicated ASICs in XS readouts enables compact and low power configurations, which are being developed for future NASA astrophysical instrumentation [35]. The spatial resolution of XS detectors has been improved to match the present MCP geometries allowing event localization as accurate as the MCP inter-pore spacing of $\sim 7\text{--}10$ μm [37]. The counting rates of these detectors was improved to multi-MHz levels and active areas as large as 10×10 cm^2 are available for such readout anodes [35,38], Fig. 5. If incoming events are spatially separated such that different strips are excited on the XS anode in both axes, several simultaneous particles can be detected.

The spatial resolution and good image linearity of 10×10 cm^2 detector with Cross Strip readout is shown in Fig. 6. The timing resolution of XS detectors was optimized for the self-triggered event detection mode with both timing and spatial information provided by the signal from the anode itself. The shaping time of the preamplifier ASICs implemented for XS event encoding was ~ 50 ns with noise level of ~ 1000 electrons rms. The timing measured by this system triggered on a signal crossing a specific threshold value has a strong dependence on the amplitude of the event, as shown in Fig. 7. The larger is the event gain the sooner it crosses the threshold, introducing the detector walk. For a narrow range of gain values the resolution was as good as 1.1 ns FWHM. With the introduction of a Constant Fraction Discrimination (CFD) into the data analysis, the dependence on the event gain was

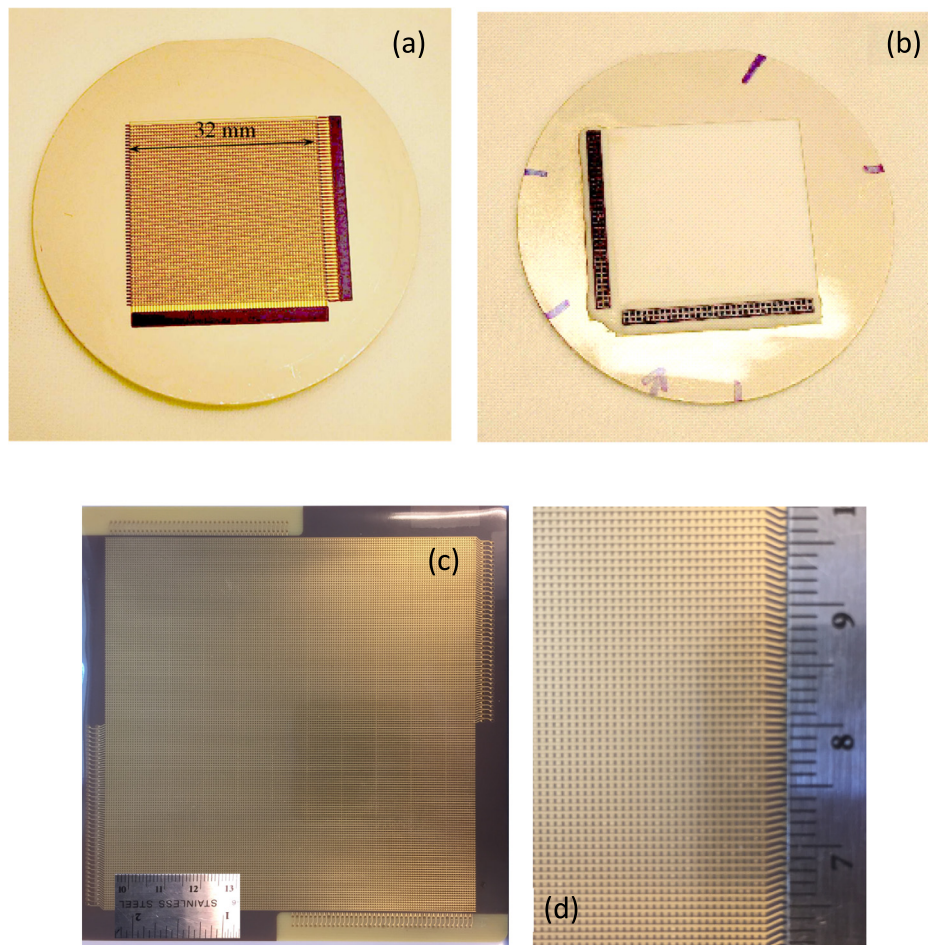


Fig. 5. (a), (b) Photographs of XS readout anode for a ~ 30 mm active area detector. Anode is implemented on a ceramic substrate compatible with the sealed tube manufacturing process. The sealed vias transfer signals from the vacuum side to the connector on the air side of the anode seen in image (b). (c), (d) — XS anode for a 10×10 cm² detector. Excellent geometric linearity of fingers is maintained over the entire area of the readout, enabling imaging with low distortions, as seen in detector images shown in Fig. 6.

eliminated and the timing accuracy of the detector improved to ~ 1.1 ns FWHM for all events above the noise threshold, when operating at a detector gain of $\sim 10^6$ [39].

3.3. Charge propagation encoding readouts

One of the most widely used readout encoding for the MCP detectors is Cross Delay Line (XDL) anode [40], where the time delay between two ends of a propagation line is measured to reconstruct the event position. The highest resolution and simplest readout electronics are implemented with a serpentine delay line, one per axis, as shown in Fig. 2b. Only four preamplifiers and two Time to Digital Converters (TDCs) are required for the detector operation [40], Fig. 8. Different formats were implemented for XDL detectors starting from small ~ 30 mm diameter active area and extended to areas as large as 20×20 cm² [41]. The small number of electronics channels allows operation of XDL detectors with flexible biasing configurations. The input of the detector can be set to any potential, for example at ground potential for the detection of low energy electrons. The output signals in such devices are capacitively coupled to the readout electronics, thus allowing the anode to be floated at any desired potential [42]. Detection of electrons with energies less than ~ 3 keV is very difficult to implement for the readouts with many output channels connected to the sensitive charge or time sensing amplifiers and digitizers (e.g. as in case of XS or Timepix readout described in next section). Multi-channel capacitive coupling (e.g. 128 channels for the XS readout) of the sensitive electronics in such readouts is very difficult to implement

in practice taking into account strict requirements on the readout noise and ~ 3 keV required potential difference across each capacitor.

The spatial resolution of XDL detectors is usually ~ 20 – 30 μm for the devices with smaller than 50×50 mm² active area and is ~ 100 μm for the large area detectors with 20×20 cm² XDL anodes [41]. One of the attractive features of XDL readouts is their capability to encode events in a very large area with relatively small distortions, which are minimized by a careful design and manufacturing of the anode electrodes, as demonstrated in Fig. 9. The counting rate of those detectors is usually limited to $< \sim 0.5$ MHz per entire detector as only one event at a time can be processed by the XDL anode. An interesting methodology was suggested for the detection of several nearly simultaneous particles, as long as they are spatially separated from each other by several mm distance [43]. If two events arrive within the time required for the processing of one event (typically it is ~ 300 ns), it is difficult to distinguish which signal at one end corresponds to the signal on the other end of that delay line as two signals arrive at each end of the delay line. That ambiguity can be eliminated by the introduction of a start trigger signal for the event arrival, which is generated from the voltage pulse at the MCP output electrode when an electron avalanche leaves the MCPs. The sum of two time delays measured at the two ends of the delay line relative to the start signal should always be equal to the propagation time of a particular anode (typical propagation time of an XDL anode is usually in 20 to 100 ns range, depending on the size of the anode). That constant time is used to distinguish which pulse on one side of the delay line corresponds to the signal on the other side of the same delay line, allowing a few simultaneous particles to be detected. The time of signal arrival at the two ends of the anode

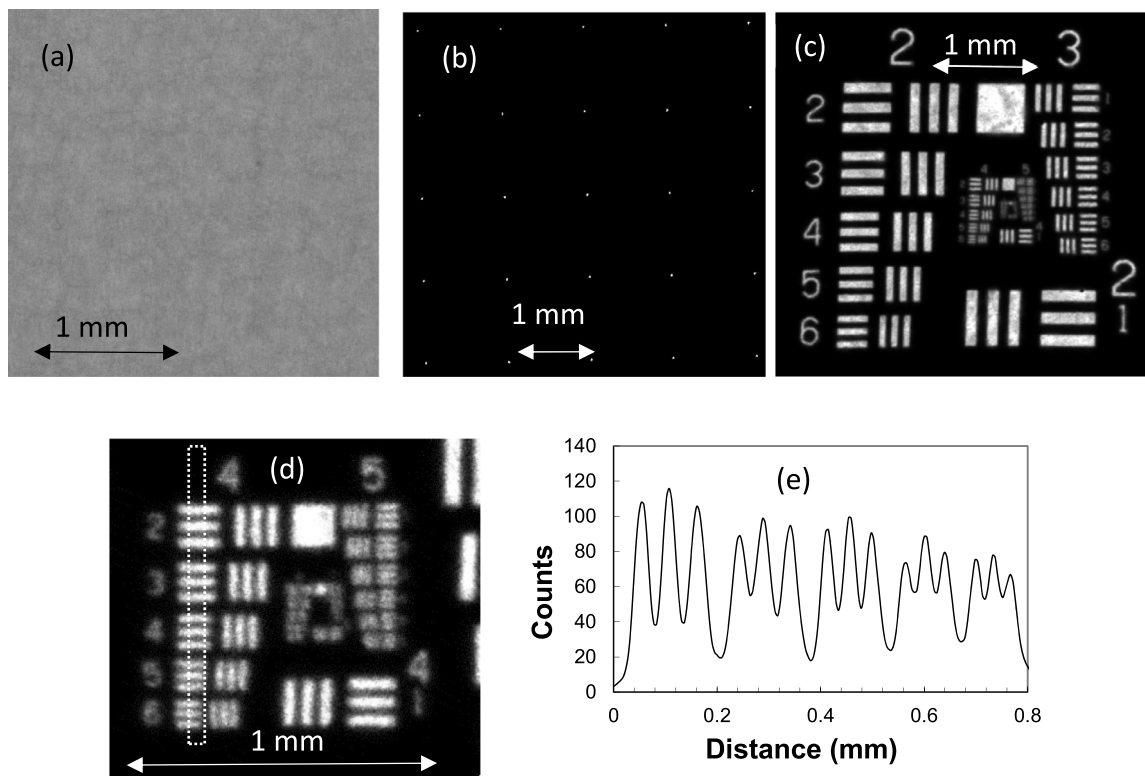


Fig. 6. UV photon images acquired with a Cross Strip readout of $10 \times 10 \text{ cm}^2$ area shown in Fig. 5c, d. (a) Deep flat field image exhibiting small residual fixed pattern modulation (at $\sim 5\%$ level) caused by the non-ideal geometry of microchannel plates: the pores typically form a hexagonal periodic pattern with some small distortions, caused by the manufacturing process, described in detail in Section 3 of reference [1]. (b) Pinhole mask image. The pinholes are $10 \mu\text{m}$ in diameter. Good linearity (with deviations less than $\sim 50 \mu\text{m}$) across the entire field of view was observed both for the flat field and for the pinhole mask images. (c), (d) US Airforce test pattern image for groups 2–5 (c) and groups 4 and 5 (d). The Dashed rectangle indicates the cross section through group 4 shown in (e). MCP chevron stack with $10 \mu\text{m}$ holes placed on a hexagonal pattern with $12.5 \mu\text{m}$ spacing between the pores is used in this experiment.

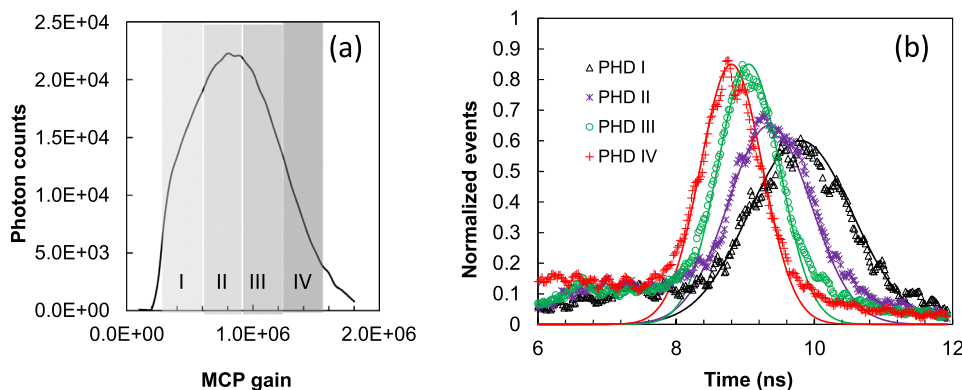


Fig. 7. Timing resolution of MCP sealed tube detector ($\sim 30 \text{ mm}$ active area) with XS readout [39]. (a) Pulse height distribution of detector. The shaded areas I–IV indicate the detector gain values for the events filtered for the reconstruction of event timing. The large gain events cross the charge threshold earlier. Gain correction can be applied to eliminate this effect in order to maintain the highest timing resolution of the detector, when timing is recovered from the pulse measured by the strips on the anode. (b) Distribution of event times measured by XS anode for different gain values of the event. Short laser pulses ($< 30 \text{ ps}$ time jitter) illuminated the detector. The timing of individual photons was measured relative to laser trigger. These data indicate that a $\sim \text{ns}$ timing resolution is possible for this self-triggered readout with a proper timing correction for the event gain.

is usually measured with 10–20 ps accuracy resulting in the spatial resolution of XDL anodes in 20–40 μm range for a typical $\sim 40 \text{ mm}$ active area. The same signal picked up at the MCP output electrode (through a decoupling capacitor) is usually used for the timing of the registered event, as shown in Fig. 2b. The event timing resolution of XDL detectors was demonstrated to be on the scale of 100–130 ps FWHM for the detection of single soft X-ray photons [44], and as low as 42 ps FWHM for electrons [45], while the detection of multiple simultaneous photons dispersed over multiple pores should enable a better timing resolution by averaging the event transit time spread over several pores. Fig. 10

shows the measurement performed with an XDL detector with active area of $\sim 30 \text{ mm}$, illuminated by the soft X-rays of $\sim 500 \text{ eV}$ energy generated at the Advanced Light Source (ALS) at Lawrence Berkeley National Laboratory. The photon bunches produced with time delay of 2 ns are seen in Fig. 10a. Please note the logarithmic scale on Y-axis in that figure, emphasizing the capability of MCP detectors to measure peaks with only few counts in them (not arriving simultaneously) due to very low readout and background noise. It should be pointed out here, that the efficiency of detection of these low intensity peaks is reduced by the presence of the preceding bright peak due to the detector dead

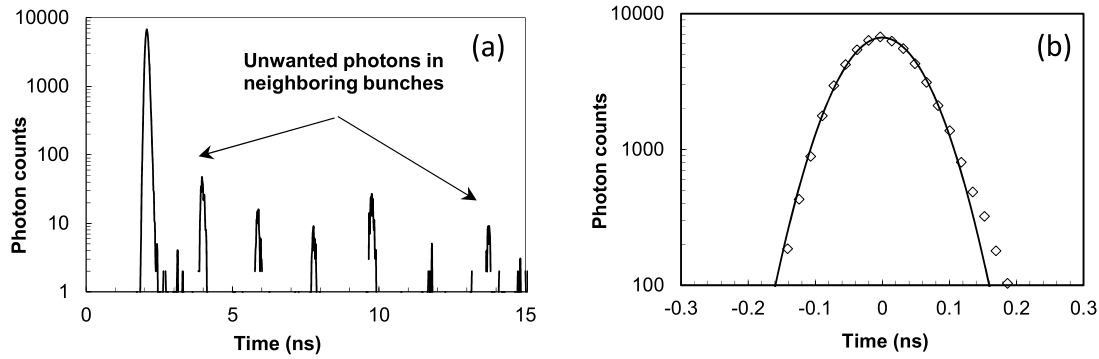


Fig. 10. Timing resolution of XDL detector measured with soft X-ray photons at the Advanced Light Source at Lawrence Berkeley National Laboratory [44]. (a) Time histogram of photon pulses registered with the XDL detector when synchrotron operated in a two-bunch mode. This graph demonstrates that MCP event counting detectors are capable of registration of the bright peak at ~2 ns simultaneously with the much dimmer subsequent peaks, although the efficiency of the subsequent peak detection is affected by the detector dead time. (b) Zoomed in strongest peak seen at 2 ns (markers) and a Gaussian fit with 55 ps rms value (solid line).

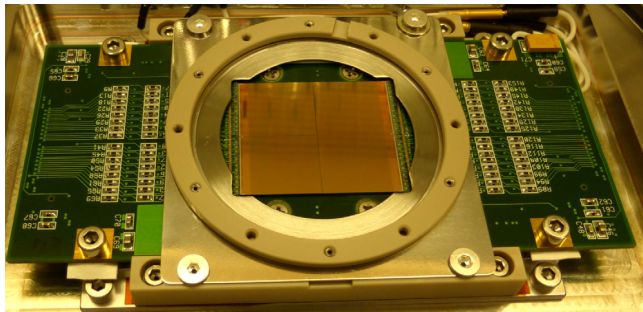


Fig. 11. Photograph of an MCP/Timepix detector with 2 × 2 array of Timepix chips visible in the center. The microchannel plates are not installed in the detector exposing the bare Timepix chips mounted at ~0.5 mm distance from the MCP stack. The detector is mounted on a conflat vacuum flange, with output signals transferred outside of vacuum on the back side of that flange.

the visible light sensors, driven by the consumer products. Combination of such sensors with microchannel plate multipliers, on one hand, extends the range of sensitivity of those sensors to other wavelengths, such as soft X-ray and UV photons and neutrons and in many cases allows operation at much lower input fluxes, including single event counting modes. Image intensifiers with the light produced at the phosphor screen, mentioned earlier, are among the possible solutions. One of the examples of high resolution detector with an image intensifier was the use of Charge Coupled Devices (CCDs) coupled to an MCP image intensifier [53,54]. Among the advantages of such readout configuration is the very small pixels in CCD produced with a lithographic accuracy and the possibility to detect many simultaneous particles with high spatial resolution, down to single MCP pore limit. Timing resolution of an MCP Intensifier coupled to a CCD detector is obviously orders of magnitude slower compared to the intrinsic capability of MCPs.

Direct coupling of a charge sensing ROIC installed directly behind MCPs in vacuum eliminates extra conversion of electrons into light and allows an immediate detection of the MCP output charge, without afterglow or afterpulsing present in some readout configurations

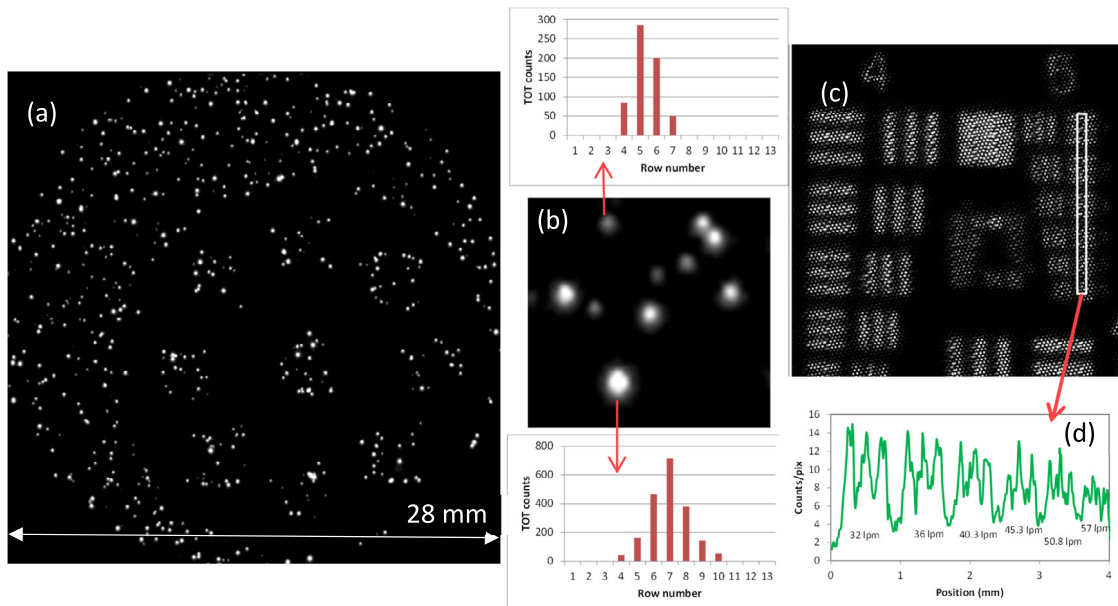


Fig. 12. UV photon images acquired by an MCP/Timepix detector operating in event centroiding mode. (a) A single frame where individual photon events are seen. The frame acquisition length is optimized to prevent event overlaps for the accurate cluster analysis required for the event centroiding. (b) Zoomed version of image (a) showing the spread in cluster size caused by MCP operation in non-saturated mode at low gain of $\sim 10^5$. The center of each cluster is found in both X and Y axes. (c) The image of an US Airforce test pattern (groups 4–6) where individual MCP pores positioned on $\sim 12 \mu\text{m}$ center-to-center spacing are resolved. The detector resolution is limited by the size of MCP pores, while the readout can encode each photon with few μm spatial resolution. (d) Cross section through the area of Group 5 in image (c) indicated by a rectangle.

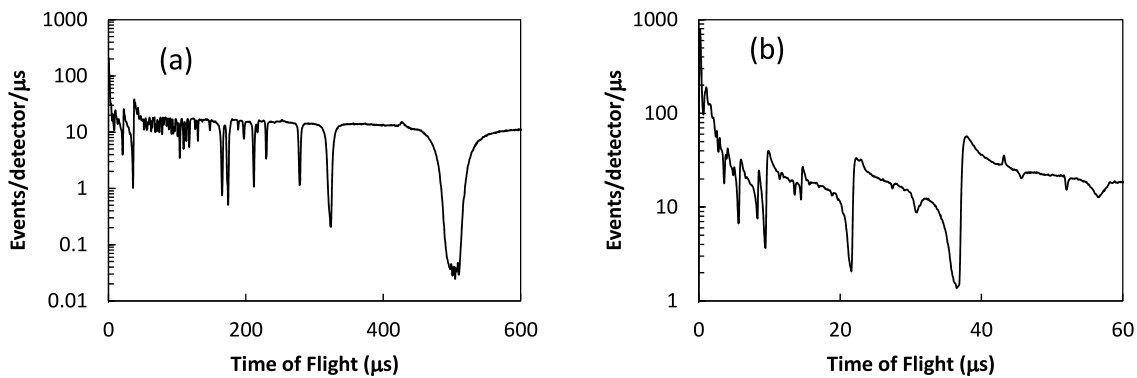


Fig. 13. Time histograms incoming neutron flux measured with the MCP/Timepix detector at a spallation neutron source. The time of neutron arrival relative to the time of spallation is measured in this experiment. The dips in the measured neutron intensity correspond to neutron energies where resonance absorption of filter materials reduces the intensity of incoming neutron beam. Many nearly simultaneous events arrive at the detector within first few μs after the spallation. (b) Zoomed in time distribution of measured neutron flux showing exponential decay of incoming flux at first few μs . Many individual neutron pulses are registered to acquire sufficient statistics. The capability to register time and position of multiple nearly simultaneous neutrons is crucial for such neutron energy-resolved imaging experiments [55].

where light conversion is involved. Medipix readout chips as well as ROICs produced by the Istituto Nazionale di Fisica Nucleare, with 55 and 50 μm pixels, respectively, were tested in combination with microchannel plate electron multipliers [56,57]. The very small capacitance of each pixel in these readouts, which enables very low internally generated noise on the scale of 50–75 e rms. A reliable event counting with low readout noise is achieved when the event gain is above the low level threshold of the readout, which in turn is set up to be well above the internal electronics noise. Thus 50–75 e rms noise level in Timepix readout enables MCP operation at a very low gain of 10^4 – 10^5 , one to two orders of magnitude lower than in XS and XDL readouts, for example. That low gain operation of MCP detectors is beneficial for the faster recovery of charge extracted from the MCP pore (making pore ready for the next incoming event and thus enabling higher local count rates). On the other hand, low gain MCP operation also increases the lifetime of the detector, which is often limited by the amount of total charge, which can be extracted from the MCP pore (there are other lifetime limiting factors such as damage due to ion feedback to a photocathode in sealed tube devices). The so-called MCP “ageing” or “scrubbing” effect results in the reduction of MCP gain, with typical lifetime limit of ~ 1 Coulomb/cm² for conventional MCPs, recently improved to at least 10 Coulomb/cm² [58] for the novel MCP manufacturing technology based on Atomic Layer Deposition [59].

One of the main advantages of such pixelated readouts is the possibility to detect a very large number of simultaneous events in event counting mode. The time resolution of both these readouts was limited to the length of the acquisition shutter, which can be controlled to few μs accuracy, followed by a readout dead time of the detector. A true event counting device with timing information for each registered particle becomes available with the introduction of Timepix ROIC [60] developed within the Medipix collaboration. One of the hardware implementations of such MCP/Timepix detector is shown in Fig. 11, where an array of 2×2 Timepix chips is seen with an MCP flange mounted above it (no MCPs are installed in that photograph). A large number ($>250,000$) of nearly independently operating pixels in that detector substantially extend the counting rate capability (up to $\sim\text{GHz}$ levels) of such event counting devices compared to charge division or charge propagation readouts. The spatial resolution of MCP/Timepix detector was demonstrated to be ~ 7 μm , limited by the MCP pore size (pore center to center distance, to be more precise, which is typically 7.2 μm for a 6 μm pore MCP and 6 μm for 5 μm pore commercial MCPs). That sub-pixel resolution is achieved through event centroiding [61], where event position is reconstructed by calculating the center of each cluster, corresponding to a single particle detection, as demonstrated in Fig. 12. In that mode of operation the MCP output charge is spread over several pixels by reducing the accelerating field or increasing the distance between the MCP and the Timepix readout. The fact

that several pixels (ideally around 9) are activated for each particle when centroiding is implemented, obviously, reduces the total counting rate capability of the MCP/Timepix detector to ~ 10 MHz levels. The next generation event driven Timepix3 readout substantially extends counting rate capability of MCP/Timepix3 detector also allowing high spatial resolution and ~ 1.6 ns timing for each registered particle, while Timepix ROIC only allows either event centroiding or event timing with 10 ns resolution. The next generation of Timepix readout (Timepix4), which is being developed within the Medipix collaboration [62] is expected to allow timing resolution of ~ 200 ps per each detected particle within the same 55 μm pixels.

The possibility to time tag each particle, many of them at the same time, make the MCP/Timepix detectors very attractive for the applications where a large number of simultaneous or nearly simultaneous events need to be registered. Among such applications are energy-resolved neutron imaging experiments at spallation neutron sources [55], where a large number of neutrons and gamma photons are produced at the time of spallation. Many particles arrive at the detector within a short time interval (few μs to milliseconds) after the spallation and need to be registered by the detector in imaging experiments where the energy of each neutron is calculated from its Time of Flight (TOF) between the spallation target and the detector, usually positioned at 7–20 m distance from the source. An example of measured neutron spectra in such experiments is shown in Fig. 13. Very important here is the fact that in one experiment $>250,000$ spectra are measured at the same time by an MCP/Timepix system, enabling many unique non-destructive testing investigations in applications as wide as materials science, engineering studies of residual strains and texture, energy research, studies of museum objects and many others [55]. Simultaneous measurement of so many transmission spectra, each within small area (down to 55 μm –size of the detector pixel) enables high resolution mapping of various sample properties, such as microstructure (through the analysis of Bragg edges for polycrystalline or Bragg dips for single crystal materials), elemental composition (through the analysis of neutron resonance absorption). These techniques provide complementary (and sometimes unique) information in addition to point by point scanning methods such as X-ray or neutron diffraction.

4. Summary

As stated earlier, there is no one type of readout configuration which best fits all the requirements and challenges of various applications utilizing event counting detectors with microchannel plates. Very frequently just one characteristic of a particular detector makes it unusable for a given experiment, despite the fact that the rest of the performance parameters are perfectly matched to the requirements. Just a simple example: an MCP/Timepix detector which can image

Table 1
Summary of MCP detector characteristics for different types of readout.

	Spatial resolution	Temporal resolution 1 particle	Global count rate	Size	MCP-Gain	Uniformity / linearity	Simultaneous events
Phosphor screen	100 μm	> 1 ms ~ns gated mode ^a	> GHz	<10 cm	10^3	Good	$\sim 10^9$ no counting ^b
Wedge Strip Zig (WSZ)	100–200 μm	10–100 ps rms	< ~ 0.5 MHz	<10 cm	10^7	Moderate	1
Cross Delay Line (XDL)	~ 20 μm (for < $\sim 4 \times 4$ cm^2 area) ~ 100 μm (for < 20×20 cm^2 area)	10–100 ps rms	< ~ 1 MHz	<20 cm	10^7	Good	1–5 ^d
Cross Strip (XS)	~ 7 –10 μm	10–100 ps MCP _{out} ~ 1.1 ns anode	~ 5 MHz	<10 cm	10^6	Small fixed pattern	1–5 ^e
Timepix	55 μm (up to GHz rates) ~ 7 μm (< 10 MHz rates)	10 ns	\sim GHz @ 55 μm ~ 10 MHz @ ~ 7 μm	$2.8 \times (2.8^*N)$ cm^2	10^5	Good, except chip gaps ^c	$\sim 10^4$
Timepix3	55 μm (up to GHz rates) ~ 7 μm (< 30 MHz rates)	0.75 ns rms	\sim GHz @ 55 μm ~ 10 MHz @ ~ 7 μm	$2.8 \times (2.8^*N)$ cm^2	10^5	Good, except chip gaps ^c	$\sim 10^4$
Timepix4 (expected)	55 μm (up to GHz rates) ~ 7 μm (< 100 MHz rates)	~ 200 ps	~ 2 GHz @ 55 μm ; ~ 200 MHz @ ~ 7 μm	$(2.8^*M) \times (2.4^*N)$ cm^2 – 4 side buttable ^f	10^5	Good, except chip gaps ^c	$\sim 10^4$
Transmission line (LAPPD)	1–3 mm	~ 100 ps rms	~ 100 MHz	<20 cm	10^7	Some distortions	1–5 ^e

^aGated mode resolution per acquisition frame, followed by a readout dead time, determined by the integrating frame readout sensor.

^bCombined with Tpx3Cam detector (Timepix-based [26]) can operate in event counting mode with $>10^6$ events/s.

^cThe dead area (gaps between the chips) is typically 50–100 μm wide.

^dFor multi-particle detection the start signal is required from the MCP_{out} electrode, the events should be separated in time by at least few ns [43].

^eEvents should be spatially separated to excite separate strips on the anode.

^fM and N are integer numbers.

photons at very high input rates, with very high spatial resolution, capable of registering multiple simultaneous events, cannot be used for the experiments where individual photon pulses, separated by 2 ns at the Advanced Light Source need to be distinguished. That is due to the fact that the timing resolution of Timepix readout is limited to 10 ns (Timepix3 allows for 1.56 ns timing and Timepix4 is expected to provide ~ 100 –200 ps resolution). Detectors with Cross Delay Line readout are being used where sub-ns time resolution is required for an imaging detector, despite their limited count rate capability. A compromise between the crucial requirements and available detector characteristics is to be found in many experiments. In Table 1 we briefly summarize the characteristics of each of the readouts described in previous sections. The values in this table are highly generalized, but can still serve as a guidance for the selection of a specific MCP detector for a particular application.

Despite all the progress in solid state photon counting devices, such as Si PMTs, detectors with microchannel plate electron amplifiers still have some niche applications where event counting with high spatial and temporal resolution over large active areas with no readout noise and high dynamic range is needed. The novel MCP manufacturing technologies and progress in the readout and data processing electronics substantially extended the counting rate capabilities and lifetime of MCP-based detectors. Therefore we believe MCP event counting devices will remain detection technology of choice for various application in the near future.

Acknowledgments

The work on the MCP detector developments at the Space Sciences Laboratory at the University of California Berkeley was partially funded through the research grants by the United States National Aeronautics and Space Administration, Department of Energy, and National Science Foundation.

References

- [1] J.L. Wiza, Microchannel plate detectors, Nucl. Instrum. Methods 162 (1979) 587–601.
- [2] J. Va'vra, D.W.G.S. Leith, B. Ratcliff, E. Ramberg, M. Albrow, A. Ronzhin, C. Ertley, T. Natoli, E. May, K. Byrum, Beam test of a time-of-flight detector prototype, Nucl. Instrum. Methods A 606 (2009) 404–410.

- [3] A. Martindale, J.S. Lapington, G.W. Fraser, Photon counting with small pore microchannel plates, Nucl. Instrum. Methods Phys. Res. A 573 (2007) 111–114.
- [4] M.J. Minot, M.A. Popecki, M.J. Wetstein, Large area picosecond photodetector (LAPPD), in: IEEE Nuclear Science Symposium Conference Record, 2018, 978-1-5386-8495-5.
- [5] O.H.W. Siegmund, N. Richner, G. Gunjala, J.B. McPhate, A.S. Tremsin, H.J. Frisch, J. Elam, A. Mane, R. Wagner, C.A. Craven, M.J. Minot, Performance Characteristics of Atomic Layer Functionalized Microchannel Plates, Proc. SPIE 8859 UV, X-ray, and Gamma-Ray Space Instrumentation for Astronomy, (2013) pp. 88590Y.
- [6] R.C. Blase, R.R. Benke, K.S. Pickens, Review of measured photon detection efficiencies of microchannel plates, IEEE Trans. Nucl. Sci. 65 (2018) 2839.
- [7] M.P. Ulmer, B.W. Wessels, B. Han, J. Gregie, A.S. Tremsin, O.H.W. Siegmund, Advances in Wide-Band-Gap Semiconductor Based Photocathode Devices for Low Light Level Applications, Proc. SPIE 5164, UV/EUV and Visible Space Instrumentation for Astronomy II, (2003) pp. 144–154.
- [8] A.S. Tremsin, O.H.W. Siegmund, The quantum efficiency and stability of UV and soft x-ray photocathodes, Proc. SPIE 5920, Ultrafast X-ray Detectors, High-Speed Imaging, and Applications; Stuart Kleinfelder, Dennis L. Paisley, Zenghu Chang, Jean-Claude Kieffer, Jerome B. Hastings; Eds, (2005) pp. 111–123.
- [9] G.W. Fraser, J.F. Pearson, The direct detection of thermal neutrons by imaging microchannel-plate detectors, Nucl. Instrum. Methods A 293 (1990) 569–574.
- [10] A.S. Tremsin, J.B. McPhate, J.V. Vallerger, O.H.W. Siegmund, J.S. Hull, W.B. Feller, E. Lehmann, Detection. efficiency, Detection efficiency spatial and timing resolution of thermal and cold neutron counting MCP detectors, Nucl. Instrum. Methods A 604 (2009) 140–143.
- [11] P. Buzhan, B. Dolgoshein, L. Filatov, A. Ilyin, V. Kantzerov, V. Kaplin, A. Karakash, F. Kayumov, S. Klemm, E. Popova, S. Smirnov, Silicon photomultiplier and its possible applications, Nucl. Instrum. Methods A 504 (2003) 48–52.
- [12] D. Renker, E. Lorenz, Advances in solid state photon detectors, J. Instrum., J. Instrum. 4 (2009) P04004.
- [13] A.C. Ulku, C. Bruschini, I.M. Antolovic, Y. Kuo, R. Ankri, S. Weiss, X. Michalet, E. Charbon, A 512 \times 512 SPAD image sensor with integrated gating for widefield FLIM, IEEE J. Sel. Top. Quantum Electron. 25 (2019) 6801212.
- [14] P. Wurz, L. Gubler, Fast microchannel plate detector for particles, Rev. Sci. Instrum. 67 (1996) 1790–1793.
- [15] J. Long, F. Furch, J. Durá, A. Tremsin, J. Vallerger, C. Schulz, A. Rouzée, M. Vrakking, Ion-ion coincidence imaging at high event rate using an in-vacuum pixel detector, J. Chem. Phys. 147 (2017) 013919.
- [16] S. Bouneau, P. Cohen, S. Della Negra, D. Jacquet, Y. Le Beyec, J. Le Bris, M. Pautrat, R. Sellem, 256-anode channel plate device for simultaneous ion detection in time of flight measurements, Rev. Sci. Instrum. 74 (2003) 57–67.
- [17] J.G. Aase, J.K. Burchill, D.J. Knudsen, J.P. Hackett, B. Moffat, Spatial resolution and relative brightness of a microchannel plate detector system with P20 and P43 phosphor screens, Opt. Eng. 50 (2011) 064001.
- [18] D.S. Hussey, J.M. LaManna, E. Baltic, D.L. Jacobson, Neutron imaging detector with 2 μm spatial resolution based on event reconstruction of neutron capture in gadolinium oxysulfide scintillators, Nucl. Instrum. Methods Phys. Res. A 866 (2017) 9–12.

- [19] J.P. Estrera, E.J. Bender, A. Giordana, J.W. Glesener, M. Iosue, Po-Ping Lin, T.W. Sinor, Long lifetime generation IV image intensifiers with unfiltered microchannel plate, *Proc. SPIE* 4128 (2000) 46–53.
- [20] S.B. Mende, H. Heetderks, H.U. Frey, M. Lampton, S.P. Geller, R. Abiad, O. Siegmund, A.S. Tremsin, J. Spann, H. Dougans, S.A. Fuselier, A.L. Magoncelli, M.B. Bumala, S. Murphree, T. Trondsen, Far ultraviolet imaging from the IMAGE spacecraft: 2. wideband FUV imaging, *Space Sci. Rev.* 91 (2000) 271–285.
- [21] I. Mor, D. Vartsky, D. Bar, G. Feldman, M.B. Goldberg, D. Katz, E. Sayag, I. Shmueli, Y. Cohen, A. Tal, Z. Vagish, B. Bromberger, V. Dangendorf, D. Mugai, K. Tittelmeier, M. Weierganz, High spatial resolution fast-neutron imaging detectors for pulsed fast-neutron transmission spectroscopy, *J. Instrum.* 4 (2009) P05016.
- [22] S.D. Pinto, R. Ortega, S. Ritzau, D. Pasquale, B. Laprade, S. Mrotek, S. Gardell, Z. Zhou, J. Plomp, L. van Eijck, H. Bilheux, I. Dhiman, Neutron imaging and tomography with mcps, *J. Instrum.* 12 (2017) C12006.
- [23] M. Fisher-Levine, A. Nomerotski, TimepixCam: a fast optical imager with time-stamping, *J. Instrum.* 11 (2016) C03016.
- [24] T. Poikela, J. Plosila, T. Westerlund, M. Campbell, M. De Gaspari, X. Llopart, V. Gromov, R. Kluit, M. van Beuzekom, F. Zappone, V. Zivkovic, C. Brezina, K. Desch, Y. Fu, A. Kruth, Timepix3: a 65K channel hybrid pixel readout chip with simultaneous ToA/ToF and sparse readout, *J. Instrum.* 9 (2014) C05013.
- [25] L.M. Hirvonen, M. Fisher-Levine, K. Suhling, A. Nomerotski, Photon counting phosphorescence lifetime imaging with TimepixCam, *Rev. Sci. Instrum.* 88 (2017) 013104.
- [26] A. Zhao, M. van Beuzekom, B. Bouwens, D. Byelov, I. Chakaberia, C. Cheng, E. Maddox, A. Nomerotski, P. Svihra, J. Visser, V. Vrba, T. Weinacht, Coincidence velocity map imaging using Tpx3Cam, a time stamping optical camera with 1.5 ns timing resolution, *Rev. Sci. Instrum.* 88 (2017) 113104.
- [27] C. Martin, P. Jeinsky, M. Lampton, R.F. Malina, H.O. Anger, Wedge-and-strip anodes for centroid-finding position-sensitive photon and particle detectors, *Rev. Sci. Instrum.* 52 (1981) 1067–1074.
- [28] O.H.W. Siegmund, M. Lampton, J. Bixler, S. Bowyer, R.F. Malina, Operational characteristics of wedge and strip image readout systems, *IEEE Trans. Nucl. Sci.* 33 (1986) 724–727.
- [29] M. Lampton, C.W. Carlson, Low-distortion resistive anodes for two-dimensional positionsensitive MCP systems, *Rev. Sci. Instrum.* 50 (1979) 1093–1097.
- [30] J.S. Lapington, Developments in imaging devices for microchannel plate detectors, in: *Proc. SPIE* 4854, Future EUV/UV and Visible Space Astrophysics Missions and Instrumentation (2003) pp. 191–202.
- [31] Y. Xing, B. Chen, H.J. Zhang, H.F. Wang, L.P. He, F.Y. Jin, Calculating and optimizing inter-electrode capacitances of charge division microchannel plate detectors, *Nucl. Instrum. Methods A* 814 (2016) 82–89.
- [32] J.F. Pearson, G.W. Fraser, C.H. Whitford, M.R.F. Siggel-King, F.M. Quinn, G. Thornton, The development of a fast imaging electron detector based on the CODACON concept, *Nucl. Instrum. Methods Phys. Res. A* 513 (2003) 183–186.
- [33] Y. Saito, S. Yokota, K. Asamura, A. Krieger, High-speed MCP anodes for high time resolution low-energy charged particle spectrometers, *J. Geophys. Res. Space Phys.* 122 (2017) 1816–1830.
- [34] O.H.W. Siegmund, A.S. Tremsin, J.V. Vallerger, R. Abiad, J. Hull, High resolution cross strip anodes for photon counting detectors, *Nucl. Instrum. Methods Phys. Res. A* 504 (2003) 177–181.
- [35] O.H.W. Siegmund, C. Ertley, J.V. Vallerger, E.R. Schindhelm, A. Harwit, B.T. Fleming, K.C. France, J.C. Green, S.R. McCandliss, W.M. Harris, Microchannel Plate Detector Technology Potential for LUVOR and HabEx, in: *Proc. SPIE* 10397 (2017) UV, X-ray, and Gamma-Ray Space Instrumentation for Astronomy XX, 1039711.
- [36] A. Seljak, H.S. Cumming, G. Varner, J. Vallerger, R. Raffanti, V. Virta, A fast, low power and low noise charge sensitive amplifier ASIC for a UV imaging single photon detector, *J. Instrum.* 12 (2017) T04007.
- [37] A.S. Tremsin, O.H.W. Siegmund, J.V. Vallerger, J. Hull, Cross strip readouts for photon counting detectors with high spatial and temporal resolution, in: *IEEE Nuclear Science Symposium, IEEE Trans. Nucl. Sci.* 51 (2003); *IEEE Trans. Nucl. Sci.* 51 (2004) 1707–1711.
- [38] J. Vallerger, J. McPhate, A. Tremsin, O. Siegmund, R. Raffanti, A. Seljak, H. Cumming, G. Varner, Development of a flight qualified 100 x 100 mm MCP UV detector using advanced cross strip anodes and associated ASIC electronics, *Space Telescopes and Instrumentation 2016: Ultraviolet to Gamma Ray*, edited by Jan-Willem A. den Herder, Tadayuki Takahashi, Marshall Bautz, in: *Proc. of SPIE* 9905 (2016) pp. 99053F.
- [39] A.S. Tremsin, O.H.W. Siegmund, J.V. Vallerger, R. Raffanti, S. Weiss, X. Michalet, High speed multichannel charge sensitive data acquisition system with self-triggered event timing, *IEEE Trans. Nucl. Sci.* 56 (2009) 1148–1152.
- [40] O.H.W. Siegmund, P. Jelinsky, S. Jelinsky, J. Stock, J. Hull, D. Doliber, J. Zaninovich, A. Tremsin, K. Kromer, High-resolution cross delay line detectors for the GALEX mission, *Proc. SPIE* 3765 (1999) 429–440.
- [41] O.H.W. Siegmund, J.B. McPhate, S.R. Jelinsky, J.V. Vallerger, A.S. Tremsin, R. Hemphill, H.J. Frisch, R.G. Wagner, J. Elam, A. Mane, Large area microchannel plate imaging event counting detectors with sub-nanosecond timing, *IEEE Trans. Nucl. Sci.* 60 (2013) 923–931.
- [42] A.S. Tremsin, G.V. Lebedev, O.H.W. Siegmund, J.V. Vallerger, J.B. McPhate, Z. Hussain, High resolution detection system for time of flight electron spectrometry, in: *Synchrotron Radiation Instrumentation (SRI 2007) Conference*, Baton Rouge, La, 2007, *Nucl. Instr. Meth. A* 526 582 (2007) 172–174.
- [43] O. Jagutzki, V. Mergel, K. Ullmann-Pfeger, L. Spielberger, U. Spillmann, R.D. Orner, H. Schmidt-Bocking, A broad-application microchannel-plate detector system for advanced particle or photon detection tasks: large area imaging, precise multi-hit timing information and high detection rate, *Nucl. Instrum. Methods Phys. Res. A* 477 (2002) 244–249.
- [44] A.S. Tremsin, O.H.W. Siegmund, J.S. Hull, J.V. Vallerger, J.B. McPhate, J. Soderstrom, J.W. Chiou, J.-H. Guo, F. Hussain, High resolution photon counting detection system for advanced inelastic X-ray scattering studies, *IEEE Trans. Nucl. Sci.* 54 (2007) 706–709.
- [45] J.A. Vredenberg, W.G. Roeterdink, M.H.M. Janssen, A photoelectron-photoion coincidence imaging apparatus for femtosecond time-resolved molecular dynamics with electron time-of-flight resolution of $\sigma = 18$ ps and energy resolution $\Delta e/e = 3.5\%$, *Rev. Sci. Instrum.* 79 (2008) 063108.
- [46] W.E. Byrne, C.-W. Chiu, J.-H. Guo, F. Sannibale, J.S. Hull, O.H.W. Siegmund, A.S. Tremsin, J.V. Vallerger, Bunch diffusion measurements at the advanced light source, in: *Proceedings of European Particle Accelerator Conference*, in: EPAC'06, Edinburgh, 2006, pp. 3466–3468.
- [47] B.W. Adams, A. Elagin, H.J. Frisch, R. Obaid, E. Oberla, A. Vostrikov, R.G. Wagner, J. Wang, M. Wetstein, Timing characteristics of large area picosecond photodetectors, *Nucl. Instrum. Methods Phys. Res. A* 795 (2015) 1–11.
- [48] M.J. Minot, B.W. Adams, M. Aviles, J.L. Bond, T. Cremer, M.R. Foley, A. Lyashenko, M.A. Popecki, M.E. Stochaj, W.A. Worstell, M.J. Wetstein, J.W. Elam, A.U. Mane, O.H.W. Siegmund, C. Ertley, H.J. Frisch, A. Elagin, E. Angelico, A. Spiegelan, Large area picosecond photodetector (LAPPD) - pilot production and development status, *Nucl. Instrum. Methods A* 936 (2019) 527–531.
- [49] M. Akatsu, Y. Enari, K. Hayasaka, T. Hokuue, T. Iijima, K. Inami, K. Itoh, Y. Kawakami, N. Kishimoto, T. Kubota, M. Kojima, Y. Kozakai, Y. Kuriyama, T. Matsuishi, Y. Miyabayashi, T. Ohshima, N. Sato, K. Senyo, A. Sugi, S. Tokuda, M. Tomita, H. Yanase, S. Yoshino, MCP-PMT timing property for single photons, *Nucl. Instrum. Methods Phys. Res. A* 528 (2004) 763–775.
- [50] K. Inami, N. Kishimoto, Y. Enari, M. Nagamine, T. Ohshima, A 5 ps TOF-counter with an MCP-PMT, *Nucl. Instrum. Methods Phys. Res. A* 560 (2006) 303–308.
- [51] D. Breton, E. Delagnes, J. Maalmi, K. Nishimura, L.L. Ruckman, G. Varner, J. Va'vra, High resolution photon timing with MCP-PMTs: A comparison of a commercial constant fraction discriminator (CFD) with the ASIC-based waveform digitizers TARGET and Wave Catcher, *Nucl. Instrum. Methods A* 629 (2011) 123–132.
- [52] S. Hirose, T. Iijima, K. Inami, D. Furumura, T. Hayakawa, Y. Kato, K. Matsuoka, R. Mizuno, Y. Sato, K. Suzuki, T. Yonekura, Development of the micro-channel plate photomultiplier for the Belle II time-of-propagation counter, *Nucl. Instrum. Methods A* 787 (2015) 293–296.
- [53] Vallerger J.V. Vallerger, O.H.W. Siegmund, J. Dalcom, P.N. Jelinsky, High-resolution (<10-um) photoncounting intensified CCD, *Proc. SPIE* 3019 (1997) 156–167, *Solid State Sensor Arrays: Development and Applications*.
- [54] K. Suhling, R.W. Airey, B.L. Morgan, Optimisation of centroiding algorithms for photon event counting imaging, *Nucl. Instrum. Methods Phys. Res. A* 437 (1999) 393–418.
- [55] A.S. Tremsin, J.V. Vallerger, Unique capabilities and applications of Microchannel Plates detectors with Medipix/Timepix readout, *subm. Nucl. Instrum. Methods A*.
- [56] J.V. Vallerger, J.B. McPhate, A.S. Tremsin, O.H.W. Siegmund, B. Mikulec, A.G. Clark, Optically sensitive Medipix2 detector for adaptive optics wavefront sensing, *Nucl. Instrum. Methods A* 546 (2005) 263–269.
- [57] R. Bellazzini, G. Spandre, M. Minuti, A. Brez, L. Baldini, L. Latronico, N. Omodei, C. Sgro', J. Bregeon, M. Razzano, M. Pinchera, A.S. Tremsin, J.B. McPhate, J.V. Vallerger, O.H.W. Siegmund, Single photon imaging at ultra-high resolution, *Nucl. Instrum. Methods A* 591 (2008) 125–128.
- [58] M. Pfaffinger, M. Böhm, A. Britting, W. Eylich, A. Lehmann, F. Uhlig, A. Ali, A. Belias, R. Dzhygadjo, A. Gerhardt, K. Götzen, G. Kalicy, M. Krebs, D. Lehmann, F. Nerling, M. Patsyuk, K. Peters, G. Schepers, L. Schmitt, C. Schwarz, J. Schwiening, M. Traxler, M. Zühlsdorf, M. Düren, E. Etzelmüller, K. Föhl, A. Hayrapetyan, K. Kreuzfeld, B. Kröck, O. Merle, J. Rieke, M. Schmidt, T. Wasem, P. Achenbach, M. Cardinali, M. Hoek, W. Lauth, S. Schlimme, C. Sienti, M. Thiel, E. Cowie, T. Keri, Recent results with lifetime enhanced microchannel-plate photomultipliers, *Nucl. Instrum. Methods A* 912 (2018) 123–127.
- [59] C. Ertley, O. Siegmund, T. Cremer, C. Craven, M. Minot, J. Elam, A. Mane, Performance studies of atomic layer deposited microchannel plate electron multipliers, *Nucl. Instrum. Methods A* 912 (2018) 75–77.
- [60] X. Llopart, R. Ballabriga, M. Campbell, L. Tlustos, W. Wong, Timepix, a 65k programmable pixel readout chip for arrival time, energy and/or photon counting measurements, *Nucl. Instrum. Methods Phys. Res. A* 581 (2007) 485–494.
- [61] A.S. Tremsin, J.V. Vallerger, R.R. Raffanti, Optimization of spatial resolution and detection efficiency for photon/electron/neutron/ion counting detectors with microchannel plates and quad timepix readout, *J. Instrum.* 13 (2018) C11005.
- [62] X. Llopart, J. Alozy, R. Ballabriga, M. Campbell, 1 N. Egidos, J.M. Fernandez, E. Heijne, I. Kremastiotis, E. Santin, L. Tlustos, V. Sriskaran, T. Poikela, Study of low power front-ends for hybrid pixel detectors with sub-ns time tagging, *J. Instrum.* 14 (2019) C01024.